

Universality in multicomponent glass-forming liquids near the glass transition

Michio Tokuyama

World Premier International Research Center, Advanced Institute for Materials Research, Tohoku University, Sendai 980-8577, Japan

(Received 25 June 2009; revised manuscript received 7 August 2009; published 11 September 2009)

The slow dynamics of a single particle in multicomponent glass-forming systems including fragile and strong glasses is studied from a unified point of view. The simulation results on two different systems, bulk glass-forming $\text{Cu}_{60}\text{Ti}_{20}\text{Zr}_{20}$ melt and network-forming SiO_2 melt are analyzed by the mean-field theory (MFT) recently proposed and are compared with other systems near the glass transition. It is shown that the simulation results for the mean-square displacement are all collapsed into a master curve given by MFT if a long-time self-diffusion coefficient has the same value in each system. It is also shown that each long-time self-diffusion coefficient is described well by a singular function predicted recently from first principles. Thus, we conclude that there exists a simple universal mechanism near the glass transition even among any diversely different glass-forming systems.

DOI: [10.1103/PhysRevE.80.031503](https://doi.org/10.1103/PhysRevE.80.031503)

PACS number(s): 64.70.P-, 66.10.C-, 61.20.Ja, 83.10.Mj

I. INTRODUCTION

Understanding of the glass transition is one of the pioneering problems encountered in a wide variety of fields, such as soft-matter science and chemical engineering, which deal with complex systems [1–4]. With recent progress in science and technology the relaxation processes of viscous liquids near the glass transition are extensively studied by experiments and computer simulations [5,6]. Several interesting statistical-mechanical theories have been also proposed to study this problem, for example, by Götze *et al.* [4,7,8] and by Medina-Noyola and co-workers [9–11]. The former work is based on a mode-coupling theory (MCT), while the latter is based on a generalized Langevin equation description. Although their approaches are limited to a calculation of two-body correlations, their results are quite successful in some cases. However, it is well known that many-body correlations play an important role near the glass transition and cause a dynamic heterogeneity [12,13]. Hence, those correlations are indispensable to discuss the slow relaxation in complex systems. In general, however, it is difficult to deal with them from first principles. In the present paper, we focus only on the dynamics of a single particle. Instead of calculating those correlations, therefore, we investigate how many-body correlations lead to universal properties in the dynamics of a single particle by just analyzing available data for the mean-square displacement from a unified point of view based on the mean-field theory (MFT) recently proposed [14,15]. We do not discuss the dynamics of the non-Gaussian parameter here since precise data are not available yet.

In this paper, we discuss whether there exists a universality near the glass transition among diversely different glass-forming systems, including fragile glass formers and strong glass formers. In the previous papers [15,16], we have shown that there exists a universality among fragile glass formers. In the present paper, we analyze the simulation results on two different systems, bulk glass-forming $\text{Cu}_{60}\text{Ti}_{20}\text{Zr}_{20}$ melt [17] and network-forming SiO_2 melt [18], from a unified point of view based on MFT and compare them with the previous results. Thus, we show that the dynamical proper-

ties of the relaxation processes in those systems are also remarkably universal as in fragile systems. The first point is that any dynamical states of the systems are uniquely determined by a long-time self-diffusion coefficient D_S^L (or a universal parameter u). The second is that any simulation results for the mean-square displacements in different systems can be described by a single master curve given by MFT at a given value of u . Thus, we show that MFT can describe not only the relaxation processes in fragile glass-forming systems but also those in strong glass-forming systems. This is also predicted from a first-principles theory recently proposed by the present author [19].

We begin in Sec. II by reviewing the theories, which are used in the present paper. In Sec. III we show the universal behavior among different systems from a unified point of view based on the MFT. We conclude in Sec. IV with a summary.

II. THEORIES

We consider three-dimensional multicomponent glass-forming systems, $A_x B_y C_z \dots$, which consists of N_α particles with mass m_α and diameter $\sigma_{\alpha\alpha}$ in the total volume V at temperature T , where $\alpha \in \{A, B, C, \dots\}$, $N = \sum_\alpha N_\alpha$, and $x + y + z + \dots = 100$. Let $\mathbf{X}_i^{(\alpha)}(t)$ and $\mathbf{P}_i^{(\alpha)}(t)$ denote the position vector of i th particle of component α and its momentum at time t .

A. First-principles theory

We first review the first-principles theory recently proposed by the present author [19]. The particle obeys the Newton equation

$$\frac{d}{dt} \mathbf{P}_i^{(\alpha)}(t) = \mathbf{F}_i^{(\alpha)}(t), \quad (1)$$

where $\mathbf{F}_i^{(\alpha)}(t)$ is a force acting on the i th particle of component α from the other particles. Equation (1) holds on the time scale of order $t_{th} (= \sigma_{\alpha\alpha} / v_{th})$, where $v_{th} [= (k_B T / m_\alpha)^{1/2}]$ is an average particle velocity.

In this paper, we are only interested in the single-particle dynamics near the glass transition, whose space-time scales are much larger than those of microscopic processes. Then, the useful physical quantities to describe the relaxation of a single particle near the glass transition are given by the self-intermediate scattering function

$$F_S^{(\alpha)}(q, t) = \langle \exp[i\mathbf{q} \cdot \{X_i^{(\alpha)}(t) - X_i^{(\alpha)}(0)\}] \rangle \quad (2)$$

and the mean-square displacement

$$M_2^{(\alpha)}(t) = \langle |X_i^{(\alpha)}(t) - X_i^{(\alpha)}(0)|^2 \rangle, \quad (3)$$

both of which are related through the relation

$$F_S^{(\alpha)}(q, t) \simeq \exp \left[-\frac{q^2}{6} M_2^{(\alpha)}(t) + \frac{q^4}{2} \left(\frac{M_2^{(\alpha)}(t)}{6} \right)^2 \alpha_2^{(\alpha)}(t) + \dots \right], \quad (4)$$

where $\alpha_2(t)$ is the non-Gaussian parameter [20].

As shown in the previous paper [19], using the Tokuyama-Mori projection operator method [21], one can transform Eq. (1) into a time-convolutionless generalized Langevin equation

$$\frac{d}{dt} \mathbf{P}_i^{(\alpha)}(t) = - \int_0^t \psi^{(\alpha)}(s) ds \mathbf{P}_i^{(\alpha)}(t) + \mathbf{f}_i^{(\alpha)}(t) \quad (5)$$

with the memory function

$$\psi^{(\alpha)}(t) = \frac{\langle \mathbf{f}_i^{(\alpha)}(t) \cdot \mathbf{f}_i^{(\alpha)}(0) \rangle}{\langle \mathbf{P}_i^{(\alpha)}(t) \cdot \mathbf{P}_i^{(\alpha)}(0) \rangle}, \quad (6)$$

where $\mathbf{f}_i^{(\alpha)}(t)$ denotes the fluctuating force and is given by

$$\mathbf{f}_i^{(\alpha)}(t) = \mathbf{F}_i^{(\alpha)}(t) + \int_0^t \psi^{(\alpha)}(s) ds \mathbf{P}_i^{(\alpha)}(t). \quad (7)$$

Here, $\mathbf{f}_i^{(\alpha)}(t)$ satisfies

$$\langle \mathbf{f}_i^{(\alpha)}(t) \cdot \mathbf{P}_i^{(\alpha)}(0) \rangle = \langle \mathbf{f}_i^{(\alpha)}(t) \rangle = 0. \quad (8)$$

The use of Eqs. (5) and (8) then leads to

$$\langle \mathbf{P}_i^{(\alpha)}(t) \cdot \mathbf{P}_i^{(\alpha)}(0) \rangle = \exp \left[- \int_0^t ds \int_0^s d\tau \psi^{(\alpha)}(\tau) \right] \langle (\mathbf{P}_i^{(\alpha)})^2 \rangle. \quad (9)$$

Equation (5) is a starting equation to discuss the dynamics of a single particle.

By using Eqs. (3) and (5), one can derive the equation for the mean-square displacement $M_2^{(\alpha)}(t)$ as [19]

$$\frac{d}{dt} M_2^{(\alpha)}(t) = 6D^{(\alpha)}(t), \quad (10)$$

where $D^{(\alpha)}(t)$ denotes the time-dependent self-diffusion coefficient and is given by

$$D^{(\alpha)}(t) = \frac{(\sigma_{\alpha\alpha} v_0) t / t_M}{1 + t \int_0^t \psi^{(\alpha)}(s) ds}. \quad (11)$$

Here, $v_0 = (\epsilon / m_\alpha)^{1/2}$ and $t_M = t_0 (v_0 / v_{th})^2$, where ϵ is an energy and $t_0 = \sigma_{\alpha\alpha} / v_0$. Let t_β denote a relaxation time of the memory function $\psi^{(\alpha)}(t)$. Then, one finds

$$M_2^{(\alpha)}(t) \simeq \begin{cases} 3v_{th}^2 t^2 & \text{for } t \ll t_\beta \\ 6D_S^L t & \text{for } t \gg t_\beta, \end{cases} \quad (12)$$

with the long-time self-diffusion coefficient

$$D_S^L = D^{(\alpha)}(t = \infty) = \frac{\sigma_{\alpha\alpha} v_0}{t_M \int_0^\infty \psi^{(\alpha)}(s) ds}. \quad (13)$$

Thus, there are different time stages, depending on time scales [14]. In an early stage (*E*) for $t \leq t_f$, the particle obeys a ballistic motion. In an intermediate stage (or β stage) (β) for $t_f \ll t \leq t_\beta$, it behaves as if it is trapped in a cage which is mostly formed by neighboring particles. This is the so-called cage effect. On the time scale of order t_β , the particles can escape their cages and in a late stage (*L*) for $t \gg t_\beta$, they obey a long-time diffusion process with D_S^L .

B. Long-time self-diffusion coefficient

In general, it is difficult to calculate the memory function up to higher order in F_i . However, this is indispensable to discuss the slow dynamics of a single particle near the glass transition because the many-body correlations play an important role near the glass transition. As shown in the previous paper [22], the long-time self-diffusion coefficient D_S^L is written as

$$\frac{D_S^L(\lambda)}{\sigma_{\alpha\alpha} v_0} = \kappa_{\alpha\alpha}^{-1} \left(\frac{\lambda_c^{(\alpha)}}{\lambda} \right) \left(1 - \frac{\lambda}{\lambda_c^{(\alpha)}} \right)^2, \quad (14)$$

where λ is a control parameter, such as an inverse temperature $1/T$ and a volume fraction ϕ , and $\lambda_c^{(\alpha)}$ is a singular point to be determined. The singular part of Eq. (14) results from the long-time correlation effects due to the many-body interactions between particles and is in general difficult to calculate. Hence, the singular point λ_c is only determined by fitting Eq. (14) with experimental data and simulation results. As is discussed later, however, there exists a universal rule to determine it.

On the other hand, the coefficient $\kappa_{\alpha\alpha}$ can be calculated analytically. The use of Eqs. (13) and (14) then leads to

$$t_M \int_0^\infty \psi^{(\alpha)}(s) ds = \kappa_{\alpha\alpha} \left(\frac{\lambda}{\lambda_c^{(\alpha)}} \right) \left(1 - \frac{\lambda}{\lambda_c^{(\alpha)}} \right)^{-2}, \quad (15)$$

As discussed in the previous paper [22], the coefficient $\kappa_{\alpha\alpha}$ can be calculated analytically at lower values of λ for such systems that (i) the intermolecular force is of long range and/or (ii) the number density is nondiluted at lower λ as

$$\kappa_{\alpha\alpha} = \frac{\sigma_{\alpha\alpha}}{\epsilon} \left(- \frac{\partial U_{\alpha\alpha}^{rep}(r)}{\partial r} \right) \Bigg|_{r=\sigma_{\alpha\alpha}}, \quad (16)$$

where $U_{\alpha\alpha}^{rep}(r)$ denotes a repulsive part of the potential $U_{\alpha\alpha}(r)$. For other systems in which the control parameter is the volume fraction ϕ and the intermolecular force is of short range with a linear force range $\sigma_{\alpha\alpha}$, an analytical prediction of $\kappa_{\alpha\alpha}$ is as follows. At lower volume fractions, the two-body repulsive interactions play an important role. In the following, therefore, we only discuss those interactions. By using Eqs. (6), (7), and (9), one can then write $\psi^{(\alpha)}(t)$, up to the lowest order in $F_i^{(\alpha)}$, as

$$\psi^{(\alpha)}(t) = \frac{\langle \mathbf{F}_i^{(\alpha)}(t) \cdot \mathbf{F}_i^{(\alpha)}(0) \rangle}{\langle (\mathbf{P}_i^{(\alpha)})^2 \rangle} + O(F_i^4), \quad (17)$$

where $\langle (\mathbf{P}_i^{(\alpha)})^2 \rangle = 3m_\alpha k_B T$. It is convenient to introduce the number densities by

$$n_S^{(\alpha)}(r) = \delta(\mathbf{r} - \mathbf{X}_i^{(\alpha)}(0)), \quad (18)$$

$$n^{(\alpha)}(r) = \sum_{i=1}^{N_\alpha} \delta(\mathbf{r} - \mathbf{X}_i^{(\alpha)}(0)). \quad (19)$$

Then, the force $\mathbf{F}_i^{(\alpha)}(0)$ can be written as

$$\mathbf{F}_i^{(\alpha)}(0) = \sum_{\beta} \int d\mathbf{r}_1 \int d\mathbf{r}_2 \mathbf{F}_{12}^{\alpha\beta} n_S^{(\alpha)}(\mathbf{r}_1) n^{(\beta)}(\mathbf{r}_2), \quad (20)$$

where $\mathbf{F}_{ij}^{\alpha\beta}$ denotes the force acting on the particle i of component α from the particle j of component β . As shown in the previous paper [22], the force term $\mathbf{F}_{ij}^{\alpha\alpha}$ is only needed to determine $\kappa_{\alpha\alpha}$ at lower values of λ . In the following, therefore, we neglect the forces acting on particle of component α from particles of other components. It is convenient to introduce the dimensionless variables as

$$\hat{\mathbf{r}} = \mathbf{r}/\sigma_{\alpha\alpha}, \quad k_B T/\epsilon = 1, \quad \hat{n} = \sigma_{\alpha\alpha}^3 n,$$

$$\hat{\mathbf{F}}_{12}^{\alpha\alpha} = (\sigma_{\alpha\alpha}/\epsilon) \mathbf{F}_{12}^{\alpha\alpha}, \quad \hat{\mathbf{P}}_i^{(\alpha)} = \mathbf{P}_i^{(\alpha)}/(m_\alpha k_B T)^{1/2}. \quad (21)$$

The average distance between particles is of order $\sigma_{\alpha\alpha}/\phi^{1/3}$, while the force range is of order $\sigma_{\alpha\alpha}$. Hence, one can write

$$\hat{\mathbf{r}}_2 = \hat{\mathbf{r}}_1 + \hat{\mathbf{r}}_{21} \simeq \hat{\mathbf{r}}_1 + O(\phi^{1/3}), \quad (22)$$

$$\hat{n}^{(\alpha)}(\hat{\mathbf{r}}_2) = \hat{n}^{(\alpha)}(\hat{\mathbf{r}}_1) + \hat{\mathbf{r}}_{21} \cdot \hat{\nabla}_1 \hat{n}^{(\alpha)}(\hat{\mathbf{r}}_1) + O(\phi^{2/3}), \quad (23)$$

where $\hat{\mathbf{r}}_{21} = \hat{\mathbf{r}}_2 - \hat{\mathbf{r}}_1$. Thus, the memory integral can be written as

$$\begin{aligned} t_M \int_0^\infty \psi^\alpha(s) ds &= t_M \frac{\langle \mathbf{P}_i^{(\alpha)}(\infty) \cdot \mathbf{F}_i^{(\alpha)}(0) \rangle}{3m_\alpha k_B T} \\ &\simeq \int d\hat{\mathbf{r}}_{21} \hat{\mathbf{F}}_{12}^{\alpha\alpha} \\ &\times \int d\hat{\mathbf{r}}_1 \frac{\langle \hat{\mathbf{P}}_i^{(\alpha)}(\infty) \hat{n}_S^{(\alpha)}(\hat{\mathbf{r}}_1) \hat{\mathbf{r}}_{21} \cdot \hat{\nabla}_1 \hat{n}^{(\alpha)}(\hat{\mathbf{r}}_1) \rangle}{3} \\ &= \left[- \int_1^\infty d\hat{r}_{21} \hat{r}_{21}^3 \frac{\partial \hat{U}_{\alpha\alpha}^{rep}(\hat{r}_{21})}{\partial \hat{r}_{21}} \right] \\ &\times \left[\int d\hat{\mathbf{r}}_1 \frac{4\pi}{3} \langle \hat{n}^{(\alpha)}(\hat{\mathbf{r}}_1) \hat{\mathbf{P}}_i^{(\alpha)}(\infty) \cdot \hat{\nabla}_1 \hat{n}_S^{(\alpha)}(\hat{\mathbf{r}}_1) \rangle \right]. \end{aligned} \quad (24)$$

$$\quad (25)$$

The second part of Eq. (25) is of order 1 and corresponds to the singular part of Eq. (15). Hence, we thus find

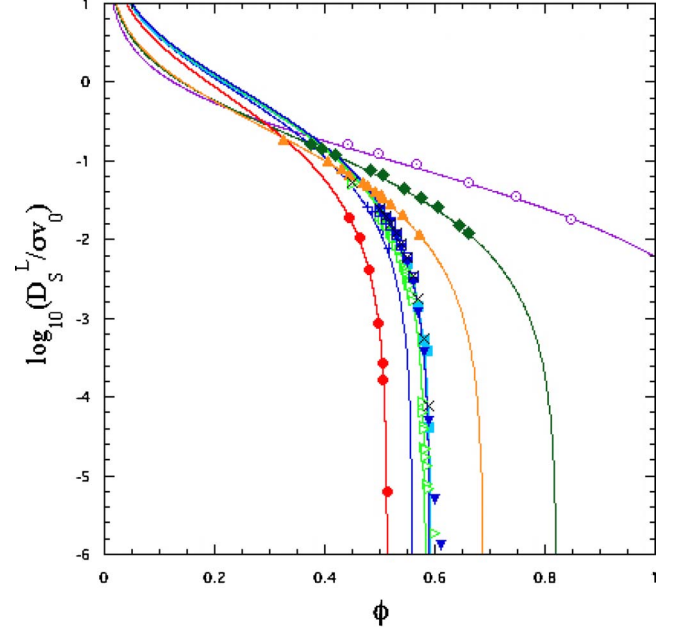


FIG. 1. (Color online) A logarithmic plot of $D_S^L/\sigma v_0$ versus ϕ for different n . The filled squares indicate the simulation results from Ref. [23] and the filled circles indicate the MCT solutions from Ref. [23] at $n=36$ and $\delta=10\%$. The other symbols indicate the simulation results: (\square) $n=36$ ($\delta=10\%$) and (\times) $n=36$ (15%) from Ref. [24], (\odot) $n=8$, (\diamond) $n=12$, (\triangle) $n=18$, (\circ) $n=36$, and ($+$) $n=144$ at $\delta=0\%$ from Ref. [25], and (\triangleright) hard spheres at $\delta=6\%$ from Ref. [27] and (∇) hard spheres at $\delta=15\%$ from Ref. [26]. The solid and the dashed lines indicate the mean-field singular function given by Eq. (14), where κ and ϕ_c are listed in Table I.

$$\kappa_{\alpha\alpha} = \int_1^\infty d\hat{r} \hat{r}^3 \left(- \frac{\partial \hat{U}_{\alpha\alpha}^{rep}(\hat{r})}{\partial \hat{r}} \right). \quad (26)$$

As a simple example, we take $U_{\alpha\alpha}(r) = k_B T (\sigma_{\alpha\alpha}/r)^{n_{\alpha\alpha}}$. Then, we obtain

$$\kappa_{\alpha\alpha} = \frac{n_{\alpha\alpha}}{n_{\alpha\alpha} - d}, \quad (27)$$

where $d=3$ here. As $n_{\alpha\alpha}$ increases, $\kappa_{\alpha\alpha}$ decreases to 1. In fact, for hard spheres where $U_{\alpha\alpha}(r)$ is given by the step function, we find $\kappa_{\alpha\alpha}=1$.

In order to test Eq. (27), we analyze the simulation results from Refs. [23–27] for the long-time self-diffusion coefficient D_S^L on the polydisperse systems of soft spheres and quasihard spheres with $\delta\%$ size polydispersity, where the potential is given by $U(r) = k_B T (\sigma/r)^n$. For comparison, the hard-sphere systems with $\delta\%$ size polydispersity are also considered. In Fig. 1, $D_S^L/\sigma v_0$ versus the volume fraction $\phi (= \pi \sigma^3 N/6V)$ is plotted for different values of n . It is thus shown that for soft spheres with $n=8$, $\kappa_{\alpha\alpha}$ is given by Eq. (16), while for quasihard spheres with $n \geq 36$ it is given by Eq. (27). On the other hand, for such systems with $9 \leq n < 36$ that they are neither soft spheres nor hard spheres, $\kappa_{\alpha\alpha}$ is only determined by fitting since there is no theory for it. The coefficient $\kappa_{\alpha\alpha}$ and the singular volume fraction ϕ_c are listed in Table I. In order to check the consistency with Eq.

TABLE I. $\kappa_{\alpha\alpha}$ and ϕ_c .

Method	n	$\kappa_{\alpha\alpha}$	ϕ_c	δ (%)	Ref.
MD	8	8 [Eq. (16)]	1.245	0	[25]
MD	12	4 (fitting)	0.822	0	[25]
MD	18	3 (fitting)	0.6885	0	[25]
MD	144	144/141 [Eq. (22)]	0.5598	0	[25]
MD	36	36/33 [Eq. (22)]	0.593	10	[24]
MD	36	36/33 [Eq. (22)]	0.593	15	[24]
MD	36	36/33 [Eq. (22)]	0.593	10	[23]
MCT	36	36/33 [Eq. (22)]	0.5136	10	[23]
MD	∞	1 [Eq. (22)]	0.583	6	[27]
MD	∞	1 [Eq. (22)]	0.5908	15	[26]

(14) more clearly, we also show a log-log plot of $D_S^L/\sigma v_0$ versus $(\phi_c/\phi)(1-\phi/\phi_c)^2$ in Fig. 2. Thus, all the simulation results are shown to be well described by Eq. (14) within errors. Finally, we note here that the simulation results on the polydisperse system with $\delta=10$ and the corresponding solutions of the MCT [23] are also well described by Eq. (14). In both cases $\kappa_{\alpha\alpha}$ has the same value as 36/33 (≈ 1.091), while the singular point ϕ_c is different from each other because the only two-body correlations are taken into account for MCT but the many-body correlations are done for the simulations. Finally, we note that the simulation results deviate from the mean-field line given by Eq. (14) at higher volume fractions. As is discussed later, this deviation always occurs around the same value of $D_S^L/\sigma_{\alpha\alpha}v_0$ even in different systems.

C. Mean-field theory

Here, we briefly summarize the MFT of the glass transition for molecular systems recently proposed by the present

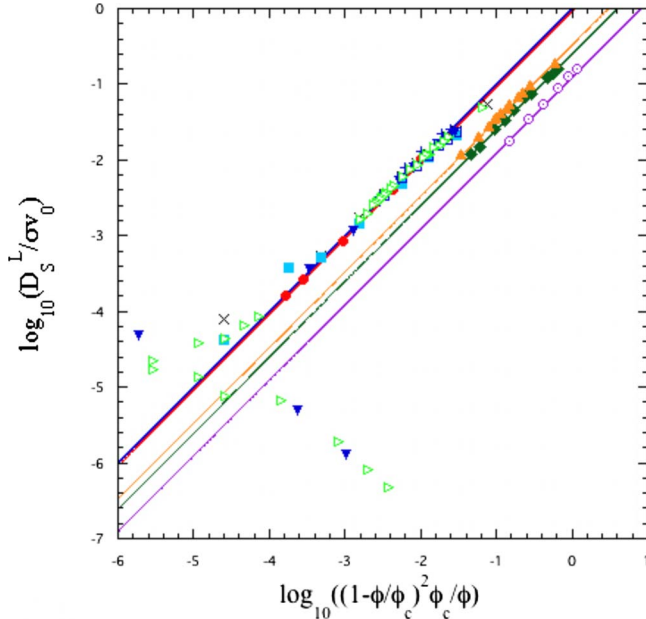


FIG. 2. (Color online) A log-log plot of $D_S^L/\sigma v_0$ versus $(\phi_c/\phi)(1-\phi/\phi_c)^2$ for different n . The details are the same as in Fig. 1.

author [14,15,28]. The mean-field theory consists of two essential points: (i) the mean-field equations for the mean-square displacement and (ii) the singular long-time self-diffusion coefficients.

Mean-field equations

The mean-square displacement $M_2^{(\alpha)}(t)$ for molecular systems is described by a nonlinear equation [14]

$$\frac{d}{dt}M_2^{(\alpha)}(t) = 6D_S^L(\lambda) + 6[v_0^2 t - D_S^L(\lambda)]e^{-M_2^{(\alpha)}(t)/\ell(\lambda)^2}, \quad (28)$$

where the mean-free path $\ell(\lambda)$ is a length in which a particle can move freely without any interactions between particles. Although it is originally related to the static structure factor $S(q)$ [28], it is determined by a fitting with data here. Equation (28) can be solve to give a formal solution

$$M_2^{(\alpha)}(t) = 2dD_S^L t + \ell^2 \ln \left[e^{-2dt/t_\beta} + \frac{1}{6} \left(\frac{t_\beta}{t_f} \right)^2 \times \left\{ 1 - \left(1 + \frac{2dt}{t_\beta} \right) e^{-2dt/t_\beta} \right\} \right], \quad (29)$$

where $t_\beta (= \ell^2/D_S^L)$ denotes a time for a particle to diffuse over a distance of order ℓ with the diffusion coefficient D_S^L and is identical to the so-called β -relaxation time. Here, $t_f (= \ell/v_0)$ is a mean-free time, within which each particle can move freely without any interactions between particles. As shown in the previous paper [15], the mean-free path ℓ is uniquely determined by $D_S^L/(\sigma_{\alpha\alpha}v_0)$. Hence, solution (29) suggests that the dynamics is described by only one parameter $D_S^L/(\sigma_{\alpha\alpha}v_0)$ if the length and the time are scaled by $\sigma_{\alpha\alpha}$ and t_0 , respectively.

Solution (29) also shows the asymptotic forms given by Eq. (12). As shown in the previous paper [14], for $\lambda \geq \lambda_s$ there exists a new time stage, the so-called β -relaxation stage (β) for $t_f \leq t \leq t_\beta$, where λ_s is a value at which a new time appears. In fact, one can find one more time scale, the caging time t_γ , as follows. First, one can obtain the following asymptotic solutions from Eq. (29):

TABLE II. Universal parameter u .

u_s	u_β	u_x	u_g
1.06	2.60	3.04	5.10

$$M_2(t) \simeq \begin{cases} \ell^2 \ln[1 + (t/t_f)^2] & \text{for } t \leq t_f \\ 6D_S^L t & \text{for } t \geq t_L, \end{cases} \quad (30)$$

where $t_L (= \sigma_{\alpha\alpha}^2 / D_S^L)$ is a long-diffusion time. We now introduce the logarithmic derivatives by

$$\varphi_1(t, \lambda) = \frac{\partial}{\partial \log t} \log |M_2(t) - \ell^2 \ln[1 + (t/t_f)^2]|, \quad (31)$$

$$M_2^{(\alpha)}(t) \simeq \begin{cases} \ell^2 \left\{ \ln \left[1 + \left(\frac{t}{t_f} \right)^2 \right] + 2 \ln \left(\frac{t}{t_\gamma} \right) + B_\gamma \left(\frac{t}{t_\gamma} \right)^{b_\gamma} \right\} & \text{for } [\beta_f], \\ \ell^2 \left\{ \ln \left[1 + \left(\frac{t}{t_\beta} \right)^2 \right] + B_\beta \left(\frac{t}{t_\beta} \right)^{b_\beta} \right\} & \text{for } [\beta_s], \end{cases} \quad (34)$$

where B_α is a positive constant and b_γ and b_β are time exponents to be determined. We mention here that in stage (β_f) the logarithmic growth dominates the dynamics for all systems since $B_\gamma \ll 1$, while in stage (β_s) the power-law growth dominates the dynamics. As λ increases, both exponents b_γ and b_β decrease and become constant as $b_\gamma = 1.0$ and $b_\beta = 1.3301$. We should note here that, since $b_\beta \geq 1$, the power-law behavior in stage (β_s) is superdiffusion type and is different from that of von Schweidler type.

The single-particle dynamics is determined by only one parameter $D_S^L / (\sigma_{\alpha\alpha} v_0)$. Hence, it is convenient to introduce a parameter u by

$$u = \log_{10}(\sigma_{\alpha\alpha} v_0 / D_S^L). \quad (35)$$

As shown in the previous paper [15], as λ is increased, the supercooled state and the glassy state appear at λ_β (u_β) and λ_g (u_g), respectively, where $\lambda_g > \lambda_\beta > \lambda_s$ ($u_g > u_\beta > u_s$). Analyses of various data show that $u_\beta \approx 2.6$, $u_g \approx 5.1$, and $u_s \approx 1.06$ (Table II). As λ increases, the time exponents b_γ and b_β decrease. In the supercooled region [S] for $u_\beta \leq u < u_g$, the exponent b_β reduces to 1.3301, while the exponent b_γ reduces to 1 in the glass region [G] for $u \geq u_g$. We should also mention here from the detailed analyses that, as u increases, the long-time self-diffusion coefficients obtained by the simulations and the experiments start to deviate from Eq. (14) at $u = u_x$ (≈ 3.04), while their mean-square displacements also show a deviation from Eq. (29) for $u > u_x$ but only in the β stage. This concurrence may not be a coincidence because the systems are considered not to be in equilibrium for $u > u_x$.

 TABLE III. SW potential parameters for $\text{Cu}_{60}\text{Ti}_{20}\text{Zr}_{20}$ from Ref. [30].

	ϵ (eV)	$c_{\alpha\beta}$	$\sigma_{\alpha\beta}$ (Å)	$R_{\alpha\beta}^c$	$n_{\alpha\beta}$
Cu-Cu	0.485	1	2.275	1.681	9
Cu-Ti		3.49484	2.300	1.794	7
Ti-Ti		3.27423	2.350	2.056	4
Cu-Zr		4.00619	2.496	1.792	8
Ti-Zr		5.61237	2.481	1.968	3
Zr-Zr		7.53608	2.646	1.855	3

III. UNIVERSALITIES NEAR THE GLASS TRANSITION

In this section, we analyze the mean-square displacements obtained in two different systems, $\text{Cu}_{60}\text{Ti}_{20}\text{Zr}_{20}$ and SiO_2 , from a unified point of view based on MFT and explore universal behavior near the glass transition. Both systems satisfy the conditions that (i) the intermolecular force is of long range and/or (ii) the number density is nondiluted at lower λ . Hence, $\kappa_{\alpha\alpha}$ is calculated from Eq. (16).

A. $\text{Cu}_{60}\text{Ti}_{20}\text{Zr}_{20}$

First, we analyze the simulation results for self-diffusion of Cu in $\text{Cu}_{60}\text{Ti}_{20}\text{Zr}_{20}$ melt [17], where $\lambda=1/T$. The

$$U_{\alpha\beta}(r) = \begin{cases} c_{\alpha\beta} \epsilon \left[\left(\frac{\sigma_{\alpha\beta}}{r} \right)^{n_{\alpha\beta}} - 1 \right] \exp \left[\left(\frac{r}{\sigma_{\alpha\beta}} - R_{\alpha\beta}^c \right)^{-1} \right] & \text{for } r < R_{\alpha\beta}^c \sigma_{\alpha\beta} \\ 0 & \text{for } r > R_{\alpha\beta}^c \sigma_{\alpha\beta}, \end{cases} \quad (36)$$

where the potential parameters are listed in Table III. Here, the total number of particles is $N=4000$. The simulation is done at 1 atm. Length, time, and temperature are scaled by σ_{CuCu} , $\sigma_{\text{CuCu}}(m_{\text{Cu}}/\epsilon)^{1/2}$, and ϵ/k_B , respectively.

In Fig. 3, the mean-square displacement $M_2(t)$ for Cu is plotted versus time t/t_0 for different temperatures. The mean-field equation given by Eq. (29) agrees with the simulation results well, except for lower temperatures $T < T_x$. Here, two adjustable parameters ℓ and D_S^L are used to fit Eq. (29) with the simulation results. For $T < T_x$ (or $u > u_x$), the simulation results deviate upward from the theoretical results only in β stage. Hence, those simulation results are considered not to reach an equilibrium state yet. As mentioned before, such a deviation always occurs at $u > u_x$. In Fig. 4, the long-time self-diffusion coefficient D_S^L is plotted versus inverse temperature. From Eq. (16), the coefficient κ_{CuCu} is calculated as $\kappa_{\text{CuCu}}=9$ [22]. The inverse singular temperature is obtained by fitting Eq. (14) with the simulation results as $1/T_c$

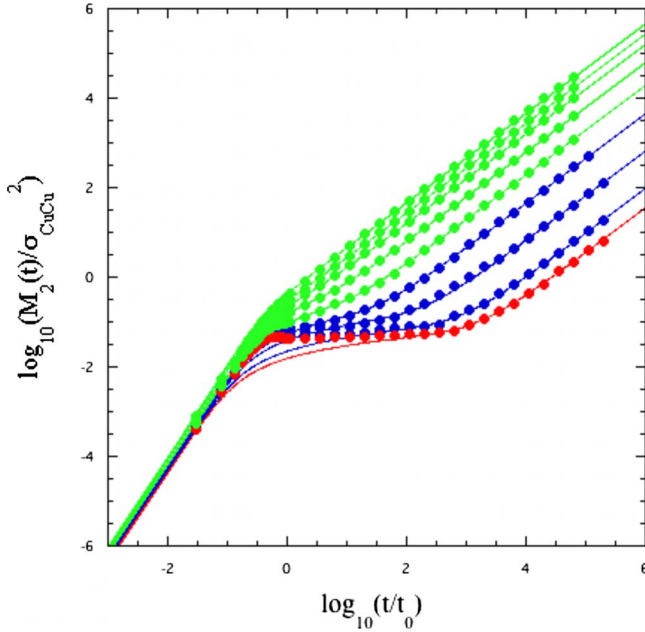


FIG. 3. (Color online) A log-log plot of $M_2^{(\text{Cu})}(t)$ versus time t/t_0 for different temperatures, $T=0.315, 0.3, 0.27, 0.23, 0.2, 0.182, 0.167, 0.154$, and 0.143 (from left to right). The filled circles indicate the simulation results for Cu from Ref. [17]. The solid lines indicate the mean-field master curve given by Eq. (29).

molecular-dynamics (MD) simulations are performed at $m_{\text{Cu}}=m_{\text{Ti}}=m_{\text{Zr}}$ by the so-called *NPT* method by using the following Stillinger-Weber potential (SW) [29]:

≈ 5.92 . Thus, Eq. (14) can describe the simulation results well, except for lower temperatures $T < T_x$ (or $u > u_x$). We note here that those simulation results also show a deviation from Eq. (14) for $u > u_x$. Hence, the simulation results do not reach an equilibrium state yet for $u > u_x$. The characteristic temperatures are listed in Table IV.

B. SiO_2

Next, we analyze the simulation results for self-diffusion of O in SiO_2 melt [18], where $\lambda=1/T$. The molecular-dynamics simulations are performed by the so-called *NVT* method by using the following potential given by Nakano *et al.* [31]:

$$U = \sum_{\alpha < \beta} U_{\alpha\beta}^{(2)} + \sum_{\alpha, \beta < \gamma} U_{\alpha\beta\gamma}^{(3)} \quad (37)$$

with the two-body potential

$$U_{\alpha\beta}^{(2)}(r) = \epsilon \left(\frac{a_{\alpha\alpha} + a_{\beta\beta}}{r} \right)^{n_{\alpha\beta}} + \frac{Z_{\alpha} Z_{\beta}}{r} e^{-r/A_0} - \frac{a_{\alpha} Z_{\beta}^2 + a_{\beta} Z_{\alpha}^2}{2r^4} e^{-r/A_1} \quad (38)$$

and the three-body potential

$$U_{\alpha\beta\gamma}^{(3)} = B_{\alpha} \exp \left[\frac{1}{r_{\alpha\beta} - A_2} + \frac{1}{r_{\alpha\gamma} - A_2} \right] \left(\frac{\mathbf{r}_{\alpha\beta} \cdot \mathbf{r}_{\alpha\gamma}}{r_{\alpha\beta} r_{\alpha\gamma}} - \cos \bar{\theta}_{\alpha} \right)^2 \theta(A_2 - r_{\alpha\beta}) \theta(A_2 - r_{\alpha\gamma}), \quad (39)$$

where $\theta(x)$ is a step function, $A_0=4.43$ (Å), $A_1=2.5$ (Å), and $A_2=5.5$ (Å). The potential parameters are listed in Table V. Here, the total number of particles is $N=5184$ and the system size is 42.8 Å. Length, time, and temperature are scaled by $\sigma_{\text{OO}}(=2a_{\text{OO}})$, σ_{OO}/v_0 , and ϵ/k_B , respectively, where $m_{\text{O}}=2.66 \times 10^{-26}$ (kg) and $\sigma_{\text{OO}}v_0=7.52 \times 10^{-7}$ (m²/s).

TABLE IV. Characteristic temperatures for Cu.

T_s	T_{β}	T_x	T_c	T_g
0.399	0.196	0.185	0.169	0.146
2247 (K)	1104 (K)	1042 (K)	952 (K)	822 (K)

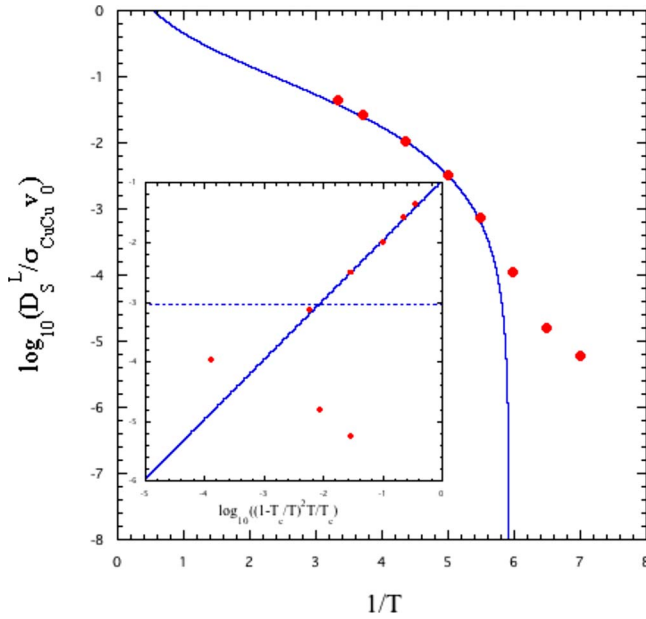


FIG. 4. (Color online) A logarithmic plot of $D_S^{L(Cu)}$ versus $1/T$. The filled circles indicate the simulation results from Ref. [17]. The solid lines indicate the mean-field singular function given by Eq. (14), where $\kappa_{CuCu}=9$ and $1/T_c=5.92$. A log-log plot of $D_S^{L(Cu)}$ versus $(T/T_c)(1-T_c/T)^2$ is given in the inset, where the dotted line indicates $-u_x$.

In Fig. 5, the mean-square displacement $M_2(t)$ for O is plotted versus time t/t_0 for different temperatures. The mean-field equation agrees with the simulation results well, except for lower temperatures $T < T_x$ (or $u > u_x$). In Fig. 6, the long-time self-diffusion coefficient D_S^L is plotted versus inverse temperature. From Eq. (16), the coefficient κ_{OO} is calculated as $\kappa_{OO}=15.31$ [22]. The inverse singular temperature is obtained by fitting Eq. (14) with the simulation results as $1/T_c \approx 6.0$. Thus, Eq. (14) can describe the simulation results well, except for lower temperatures $T < T_x$ (or $u > u_x$). This situation is the same as that discussed in Cu. The characteristic temperatures are listed in Table VI.

In order to show whether Eq. (14) holds for the other network glass formers, we analyze the data given by Hemmati and Angell for different model potentials of SiO_2 [32]. As shown in the previous paper [22], the coefficient κ_{OO} should be the same as that obtained by using Eq. (37), even though the model potentials are different. Hence, we take $\kappa_{OO}=15.31$ and $\sigma_{OO}v_0=7.52 \times 10^{-7}$ (m^2/s) to analyze seven different data discussed in Ref. [32]. In Fig. 7, we show a

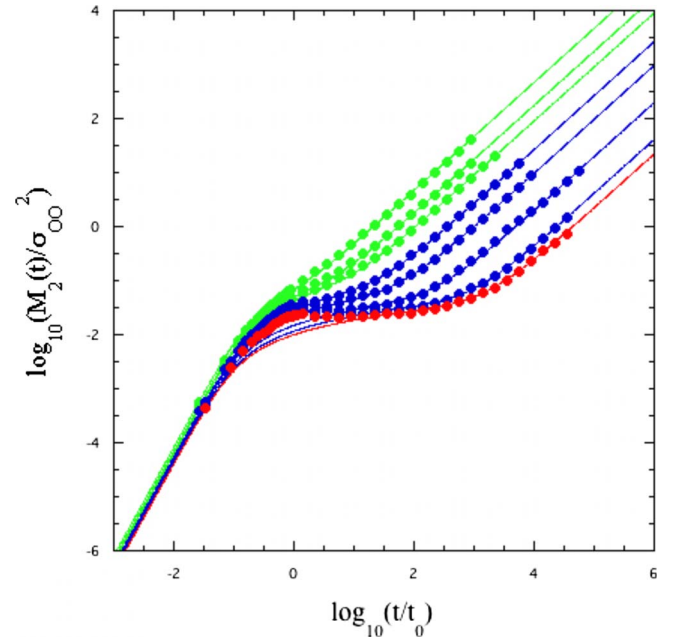


FIG. 5. (Color online) A log-log plot of $M_2^{(O)}(t)$ versus time t/t_0 for different temperatures, $T=0.2706, 0.2273, 0.2057, 0.1813, 0.1678, 0.1516, 0.1407$, and 0.1353 (from left to right). The filled circles indicate the simulation results for O from Ref. [18]. The solid lines indicate the mean-field master curve given by Eq. (29).

logarithmic plot of the oxygen self-diffusion coefficient $D_S^{L(O)}$ versus the reduced temperature T_c/T . The inverse singular temperatures are obtained by fitting Eq. (14) with the simulation results and are listed in Table VII. For comparison, the simulation results obtained by using Eq. (37) are also shown in Fig. 7. In Fig. 8, a log-log plot of $D_S^{L(O)}$ versus $(T/T_c)(1-T_c/T)^2$ is also shown to check consistency with Eq. (14). All simulation results obtained by using different potentials are well described by a single master curve given by Eq. (14) up to u_x . This is reasonable because most of those potentials have been made, so that their static structure factors describe realistic structural properties of SiO_2 . Here, we note that the potential difference appears only in the singular temperature.

C. Exponents b_β and b_γ

We now discuss the exponents b_γ and b_β obtained for $\text{Cu}_{60}\text{Ti}_{20}\text{Zr}_{20}$ and SiO_2 . They are calculated numerically from Eqs. (31) and (32) by using fitting values of ℓ and D_S^L . In Fig.

TABLE V. Potential parameters for SiO_2 .

	ϵ (eV)	$a_{\alpha\beta}$ (Å)	Z_α (e)	a_α (Å ³)	$n_{\alpha\beta}$	B_α (eV)	$\bar{\theta}_\alpha$
O-O	1.592	1.2	1.76	2.4	7		
Si-Si	1.592	0.47	-0.88	0.00	11		
O-Si	1.592				9		
O-Si-O						4.993	109.47
Si-O-Si						19.972	141.00

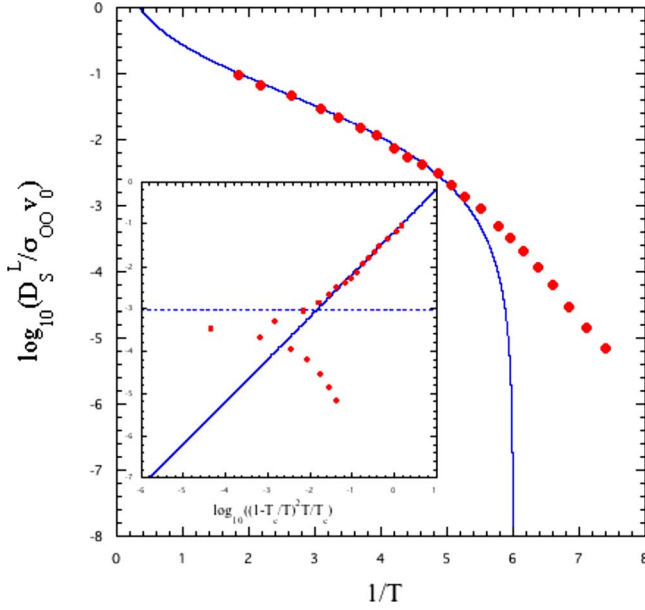


FIG. 6. (Color online) A logarithmic plot of $D_S^{L(O)}$ versus $1/T$. The filled circles indicate the simulation results from Ref. [18]. The solid lines indicate the mean-field singular function given by Eq. (14), where $\kappa_{OO}=15.31$ and $1/T_c=6.0$. A log-log plot of $D_S^{L(O)}$ versus $(T/T_c)(1-T_c/T)^2$ is given in the inset, where the dotted line indicates $-u_x$.

9, they are plotted versus u . As typical examples of fragile systems, the simulation results for the hard-sphere fluids with 15% size polydispersity [26] and 6% size polydispersity [27] and the Lennard-Jones (LJ) binary mixtures [33] are also plotted for comparison. As u increases, b_β and b_γ decrease and reduce to each the constant 1.3301 at a supercooled point u_β and 1.0 at a glass point u_g , respectively. Although the systems are completely different from each other, all their exponents coincide with each other within error. This universality is already seen in fragile systems [15].

D. Mean-free path ℓ

We next discuss the mean-free path ℓ obtained for $\text{Cu}_{60}\text{Ti}_{20}\text{Zr}_{20}$ and SiO_2 . In Fig. 10, it is plotted versus u for different systems. For comparison, the simulation results for the hard-sphere fluids and the Lennard-Jones binary mixtures are also shown. The lengths ℓ of O and Cu do not agree with other fragile systems. But if one scales ℓ of O and Cu by $1.8\sigma_{OO}$ and $1.5\sigma_{CuCu}$, respectively, then they agree with others. Those scaled fittings are needed because $\sigma_{\alpha\alpha}$ is not a diameter of O or Cu but just a technical number to make the length scale dimensionless. We note that ℓ of Cu does not agree with others in a liquid state. This would be because the

TABLE VI. Characteristic temperatures for O.

T_s	T_β	T_x	T_c	T_g
0.500	0.203	0.188	0.167	0.136
9242 (K)	3752 (K)	3475 (K)	3087 (K)	2514 (K)

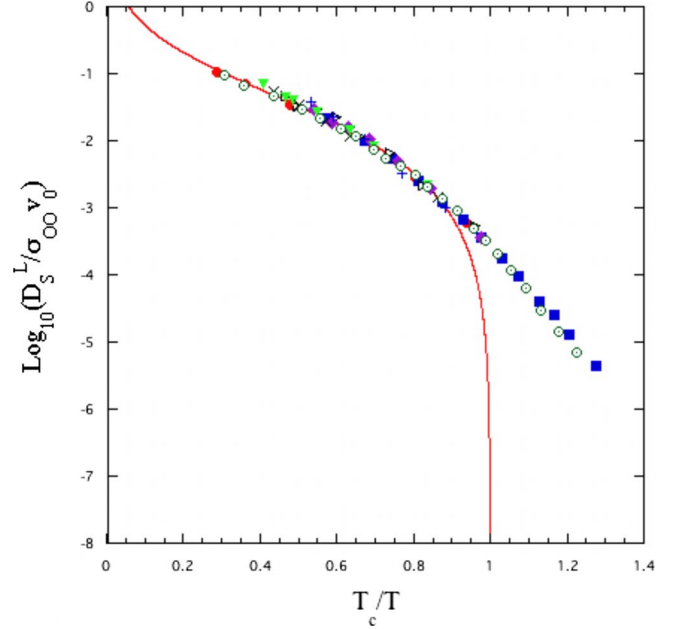


FIG. 7. (Color online) A logarithmic plot of $D_S^{L(O)}$ versus T_c/T for different models of SiO_2 . The symbols indicate the simulation results from Ref. [32], except that with the symbol (\odot) is from [18]. The solid lines indicate the mean-field singular function given by Eq. (14), where $\kappa_{OO}=15.31$ and $\sigma_{OO}v_0=7.52 \times 10^{-7}$ [m^2/s]. The singular temperatures are listed in Table VII.

simulations on Cu have been done by the *NPT* method, while the other simulations have been done by the *NVT* method.

E. Characteristic times t_β and t_γ

We also discuss the characteristic times t_β and t_γ obtained for $\text{Cu}_{60}\text{Ti}_{20}\text{Zr}_{20}$ and SiO_2 . In Fig. 11, they are plotted versus u . For comparison, the simulation results for the hard-sphere fluids and the Lennard-Jones binary mixtures are also shown. The u dependence of those times are similar to each other, where the results for O and Cu are also scaled by the times $1.8\sigma_{OO}/v_0$ and $1.5\sigma_{CuCu}/v_0$, respectively, as in Fig. 10.

F. Mapping

In this section, we discuss a dynamical mapping from one system to another at a given value of D_S^L [16]. We consider

TABLE VII. Singular temperatures for different models.

Model	$1000/T$ (K^{-1})	Symbol	Ref.
Modified-Matsui	0.350	\circ	[32]
Tsuneyuki	0.305	\triangleright	[32]
BKS	0.285	\diamond	[32]
Horbach (BKS)	0.267	\square	[32]
Poole	0.200	∇	[32]
TRIM	0.1976	\times	[32]
Kubicki	0.1905	$+$	[32]
Nakano	0.324	\odot	[31]

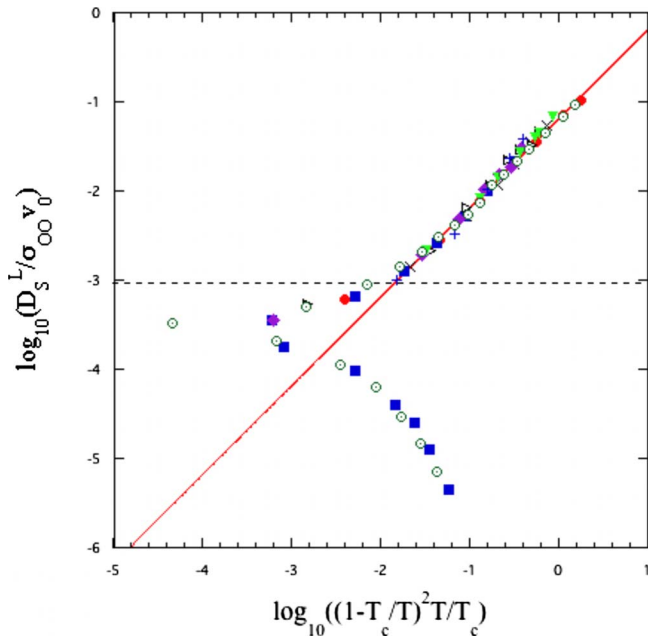


FIG. 8. (Color online) A log-log plot of $D_S^{L(O)}$ versus $(T/T_c)(1 - T_c/T)^2$. The dashed line indicates $-u_\gamma$. The details are the same as in Fig. 7.

the following three cases. The first is a mapping from Cu to the hard-sphere fluid with 6% size polydispersity (HSF6%). In Fig. 12, the mean-square displacement $M_2(t)$ is compared at two different values of D_S^L ; in a liquid state [L] at

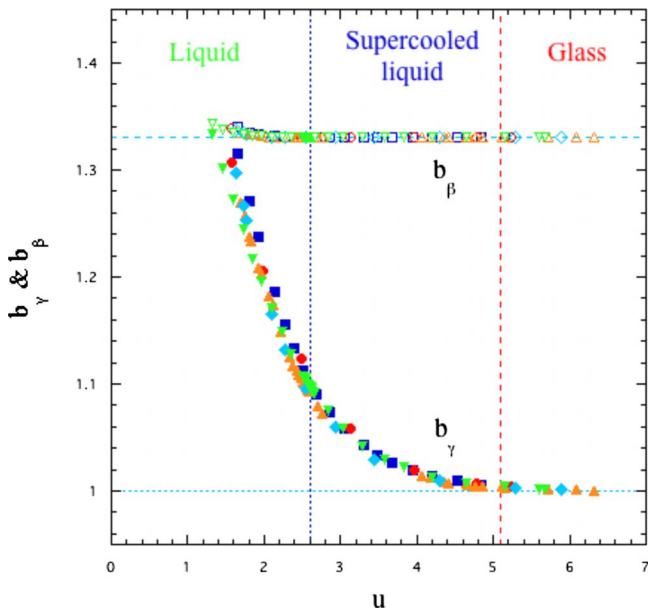


FIG. 9. (Color online) A plot of b_γ and b_β versus u for different systems. The open symbols indicate the exponent b_β and the filled symbols indicate b_γ : (O) Cu, (\square) O, (\diamond) hard-sphere fluids with 15 % size polydispersity from Ref. [26], (\triangle) hard-sphere fluids with 6 % size polydispersity from Ref. [27], and (∇) LJ from Ref. [33]. The horizontal dotted line indicates $b_\gamma=1.0$ and the horizontal dashed line indicates $b_\beta=1.33014$. The vertical dotted line indicates u_β and the vertical dashed line indicates u_g .

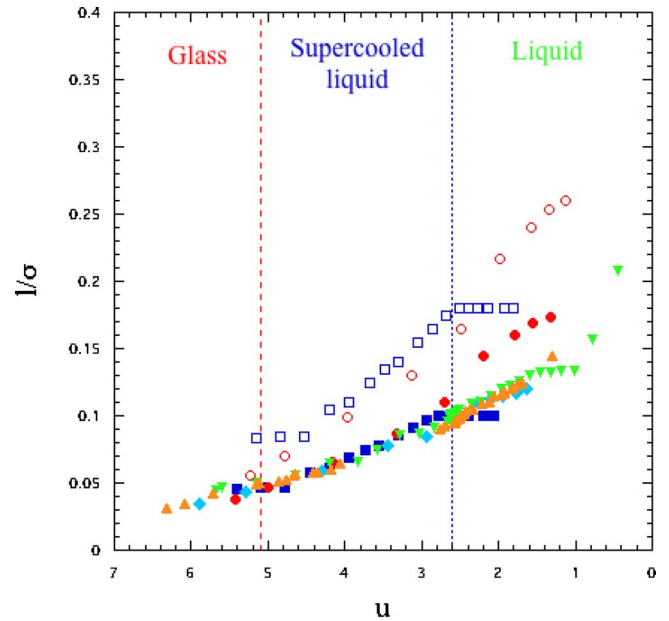


FIG. 10. (Color online) A plot of ℓ/σ versus u for different systems. The open squares and circles indicate the original results for O and Cu, respectively, and the filled squares and circles the scaled ones. The details are the same as in Fig. 9.

$D_S^L/(\sigma v_0) \approx 0.05$, where $\phi=0.45$ for the hard-sphere fluid and $T=0.27$ for Cu, and in a supercooled liquid state [S] at $D_S^L/(\sigma v_0) \approx 0.0017$, where $\phi=0.56$ and $T=0.182$. At each value the simulation results are collapsed on the mean-field master curve. Here, we note that in a supercooled state the simulation results for Cu deviate from the mean-field theory because they do not reach an equilibrium state yet.

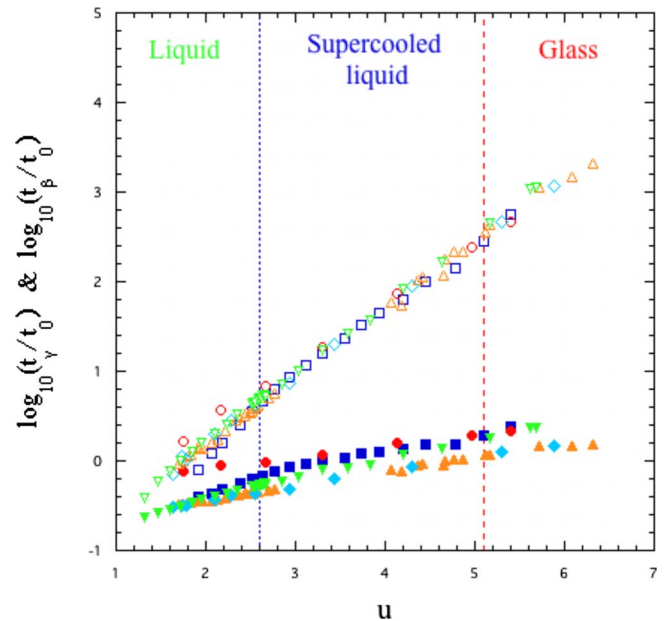


FIG. 11. (Color online) A plot of t_γ and t_β versus u for different systems. The open symbols indicate the time t_β and the filled symbols indicate t_γ . The details are the same as in Fig. 9.

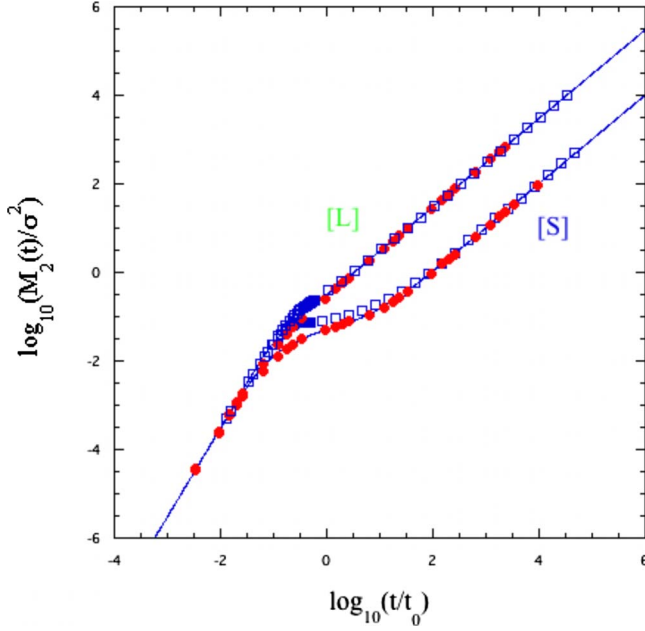


FIG. 12. (Color online) A log-log plot of $M_2(t)/\sigma^2$ versus t/t_0 for two different systems: HSF6% and $\text{Cu}_{60}\text{Ti}_{20}\text{Zr}_{20}$. The filled circles indicate the simulation results for hard spheres with 6% size polydispersity at [L] $\phi=0.45$ and [S] 0.56 from Ref. [27] and the open squares for Cu at [L] $T=0.27$ and [S] 0.182 from Ref. [17]. The solid lines indicate the mean-field master curve given by Eq. (29).

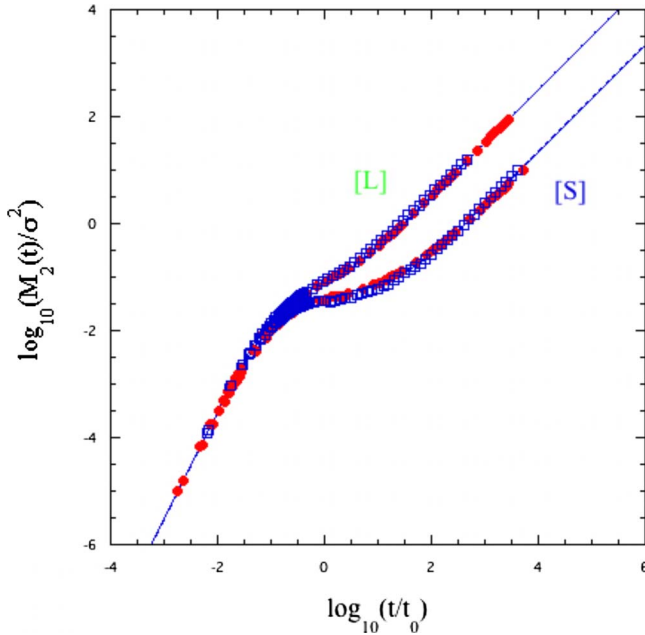


FIG. 13. (Color online) A log-log plot of $M_2(t)/\sigma^2$ versus t/t_0 for two different systems: HSF15% and SiO_2 . The filled circles indicate the simulation results for hard spheres with 15% size polydispersity at [L] $\phi=0.55$ and [S] 0.58 from Ref. [26] and the open squares for O at [L] $T=0.2273$ and [S] 0.1678 from Ref. [18]. The solid lines indicate the mean-field master curve given by Eq. (29).

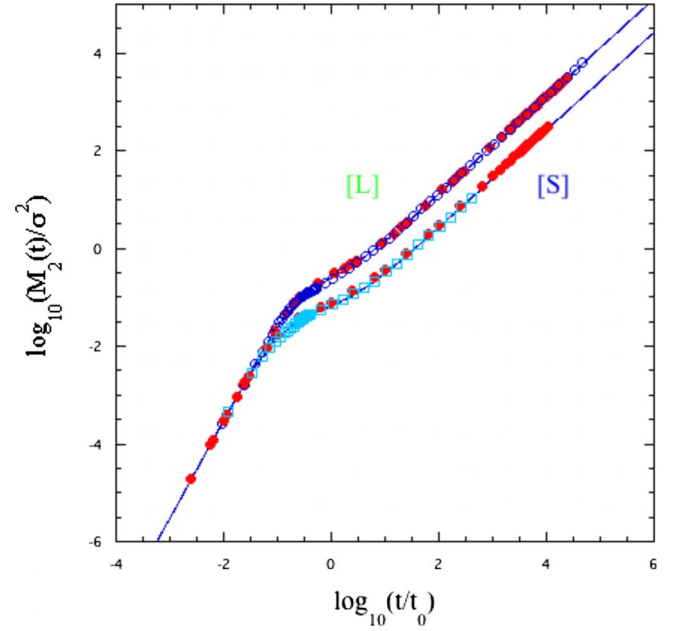


FIG. 14. (Color online) A log-log plot of $M_2(t)/\sigma^2$ versus t/t_0 for three different systems: LJ, $\text{Cu}_{60}\text{Ti}_{20}\text{Zr}_{20}$, and SiO_2 . The filled circles indicate the simulation results for LJ at [L] $T=1.0$ and [S] 0.769 from Ref. [33], the open circles for Cu at [L] $T=0.23$ from Ref. [17], and the open squares for O at [S] $T=0.2165$ from Ref. [18]. The solid lines indicate the mean-field master curve given by Eq. (29).

The second is a mapping from O to the hard-sphere fluid with 15% size polydispersity (HSF15%). In Fig. 13, the mean-square displacement $M_2(t)$ is compared at two different values of D_S^L : in a liquid state [L] at $D_S^L/(\sigma v_0) \approx 0.0053$, where $\phi=0.55$ for the hard-sphere fluid and $T=0.2273$ for O, and in a supercooled liquid state [S] at $D_S^L/(\sigma v_0) \approx 0.00036$, where $\phi=0.58$ and $T=0.1678$. At the same value of D_S^L , the simulation results are collapsed on the corresponding mean-field master curves given by Eq. (29).

The last is a mapping from O and Cu to the LJ binary mixtures. In Fig. 14, the mean-square displacement $M_2(t)$ is compared at two different values of D_S^L : in a liquid state [L] at $D_S^L/(\sigma v_0) \approx 0.01$, where $T=1.0$ for LJ and $T=0.23$ for Cu, and in a supercooled liquid state [S] at $D_S^L/(\sigma v_0) \approx 0.002$, where $T=0.769$ for LJ and $T=0.2165$ for O. At the same value of D_S^L all the simulation results on fragile and strong glass formers are collapsed on the mean-field master curve given by Eq. (29). Hence, the dynamical behavior in different systems is identical to each other if D_S^L is the same. This universality is also true even for stronger glass formers, although this was discussed only in fragile glass formers in the previous paper [16].

G. Long-time self-diffusion coefficient

Finally, we discuss the universality among the long-time self-diffusion coefficients for diversely different glass-forming systems. In Fig. 15, D_S^L is plotted versus λ/λ_c for different systems. All simulation results are described by the master curve given by Eq. (14) well, except for higher values

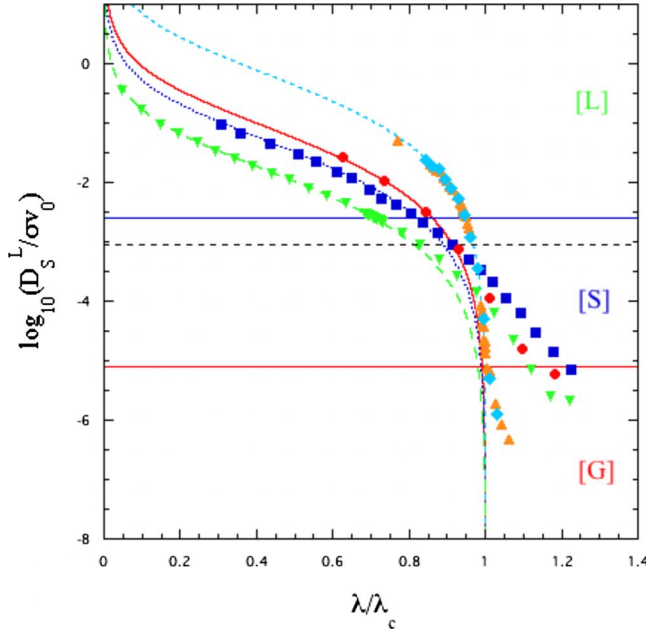


FIG. 15. (Color online) A logarithmic plot of D_S^L/σ_0 versus λ/λ_c for different systems. The solid line indicates the mean-field master curve given by Eq. (14) at $\kappa_{CuCu}=9.0$, the dotted line at $\kappa_{OO}=15.31$, the dashed line at $\kappa=1$ for hard spheres, and the long-dashed line at $\kappa=48$ for LJ. The horizontal solid lines indicate u_β and u_g , while the horizontal dashed line indicates $-u_x$. [L] stands for a liquid state $0 < u < u_\beta$, [S] for a supercooled state $u_\beta \leq u < u_g$, and [G] for a glass state $u_g \leq u$. The details are the same as in Fig. 9.

$\lambda/\lambda_x > 1$ (or $u > u_x$), where the systems do not reach an equilibrium state yet. In order to check consistency with Eq. (14) more clearly, we also show a log-log plot of D_S^L/σ_0 versus $(\lambda_c/\lambda)(1-\lambda/\lambda_c)^2$ in Fig. 16. Thus, all the simulation results are shown to be described by Eq. (14) well up to λ_x over which the deviation from Eq. (14) starts to occur. Hence, this suggests that the λ/λ_c dependence of D_S^L in any systems should be the same for $\lambda/\lambda_x \leq 1$ [22]. This is clearly seen in Fig. 17, where κD_S^L is plotted versus λ/λ_c for different systems. When $\lambda/\lambda_x > 1$ (or $u > u_x$), κD_S^L obeys a nonsingular function and its value is larger for stronger glasses. For $\lambda/\lambda_c > 1$, however, the systems are usually out of equilibrium. In order to calculate such a nonsingular function, therefore, one has to discuss the nonequilibrium relaxation processes separately from the equilibrium formulation discussed here.

IV. SUMMARY

In this paper, we have analyzed two different glass-forming systems, bulk glass-forming $\text{Cu}_{60}\text{Ti}_{20}\text{Zr}_{20}$ melt and network-forming SiO_2 melt, from a unified viewpoint based on the mean-field theory. We have first shown that the both simulation results for the mean-square displacement $M_2(t)$ are well described by the mean-field master curve given by Eq. (29), except for lower temperatures $T < T_x$ (or $u > u_x$) where the system does not reach an equilibrium state yet. We have then shown that if the long-time self-diffusion coefficient in different systems has the same value, those results

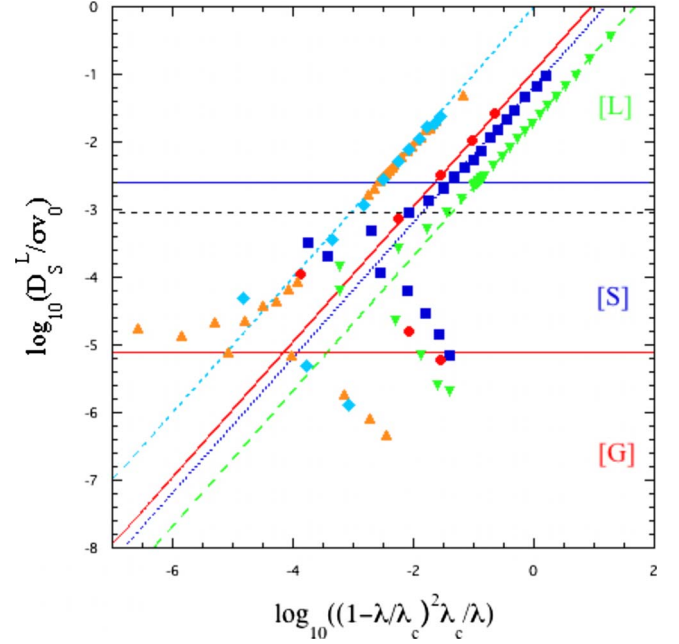


FIG. 16. (Color online) A log-log plot of D_S^L/σ_0 versus $(\lambda_c/\lambda)(1-\lambda/\lambda_c)^2$ for different systems. The details are the same as in Fig. 15. Here, the data points for $\lambda/\lambda_c > 1$ are excluded for a simplicity.

are collapsed into a master curve given by Eq. (29). Second, we have shown that the simulation results for the long-time self-diffusion coefficient D_S^L obey a mean-field singular curve given by Eq. (14) well, except for lower temperatures $T < T_x$ (or $u > u_x$). These situations are exactly the same as those discussed in fragile systems [15,16]. In fact, we have

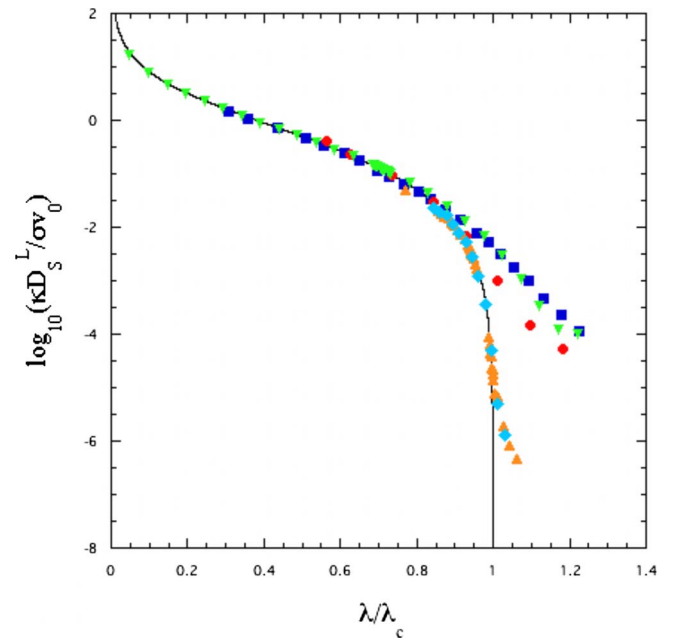


FIG. 17. (Color online) A logarithmic plot of $\kappa \times D_S^L/(\sigma_0)$ versus λ/λ_c for different systems. The solid line indicates the mean-field master curve given by Eq. (14) at $\kappa=1$. The details are the same as in Fig. 9.

compared the results with those obtained in fragile systems, such as hard-sphere fluids. Thus, we conclude that there exists a simple universal mechanism near the glass transition even among any diversely different glass-forming systems. Finally, we should mention that the mean-field theory holds only in an equilibrium state for $\lambda \leq \lambda_x$ (or $u \leq u_x$). For $\lambda > \lambda_x$ (or $u > u_x$), however, the dynamic (spatial) heterogeneity becomes more important. Hence, one has to formulate a new theory to discuss such a region. This will be discussed elsewhere.

ACKNOWLEDGMENTS

The author is grateful to H. Fujii, Y. Kimura, H. Löwen, M. Medina-Noyola, T. Narumi, I. Sasaki, A. Takeuchi, H. Teichler, Y. Terada, Th. Voigtmann, and Y.-H. Hwang for fruitful discussions. This work was supported by World Premier International Research Center Initiative, MEXT, Japan and also partially supported by Grants-in-Aid for Science Research under Contract No. 18540363 from Ministry of Education, Culture, Sports, Science and Technology of Japan.

-
- [1] C. A. Angell, K. L. Ngai, G. B. McKenna, P. F. McMillan, and S. W. Martin, *J. Appl. Phys.* **88**, 3113 (2000).
- [2] P. G. Debenedetti and F. H. Stillinger, *Nature (London)* **410**, 259 (2001).
- [3] K. Binder and W. Kob, *Glassy Materials and Disordered Solids* (World Scientific, Singapore, 2005).
- [4] W. Götze, *Complex Dynamics of Glass-Forming Liquids* (Oxford University Press, New York, 2009).
- [5] Proceedings of the 4th International Discussion Meeting on Relaxation in fragile Systems, edited by K. L. Ngai [*J. Non-Cryst. Solids* **307-310**, 1 (2002)].
- [6] *Proceedings of the 3rd International Symposium on Slow Dynamics in Complex Systems*, edited by M. Tokuyama and I. Oppenheim (AIP, New York, 2004).
- [7] U. Bengtzelius, W. Götze, and A. Sjölander, *J. Phys. C* **17**, 5915 (1984).
- [8] W. Götze, in *Liquids, Freezing and Glass Transition*, edited by J. P. Hansen, D. Levesque, and J. Zinn-Justin (North-Holland, Amsterdam, 1991).
- [9] L. Yeomans-Reyna and M. Medina-Noyola, *Phys. Rev. E* **64**, 066114 (2001).
- [10] M. A. Chávez-Rojo and M. Medina-Noyola, *Phys. Rev. E* **72**, 031107 (2005).
- [11] R. Juárez-Maldonado and M. Medina-Noyola, *Phys. Rev. E* **77**, 051503 (2008).
- [12] H. Fynewever and P. Harrowell, *Prog. Theor. Phys. Suppl.* **138**, 199 (2000).
- [13] A. Widmer-Cooper, P. Harrowell, and H. Fynewever, *Phys. Rev. Lett.* **93**, 135701 (2004).
- [14] M. Tokuyama, *Physica A* **364**, 23 (2006).
- [15] M. Tokuyama, *Physica A* **378**, 157 (2007).
- [16] M. Tokuyama, T. Narumi, and E. Kohira, *Physica A* **385**, 439 (2007).
- [17] H. Fujii, Master's thesis, Tohoku University, 2008.
- [18] I. Sasaki, Master's thesis, Tohoku University, 2008.
- [19] M. Tokuyama, *Physica A* **387**, 5003 (2008).
- [20] A. Rahman, K. S. Singwi, and A. Sjölander, *Phys. Rev.* **126**, 986 (1962).
- [21] M. Tokuyama and H. Mori, *Prog. Theor. Phys.* **55**, 411 (1976).
- [22] M. Tokuyama, *Physica A* **388**, 3083 (2009).
- [23] Th. Voigtmann, A. M. Puertas, and M. Fuchs, *Phys. Rev. E* **70**, 061506 (2004).
- [24] S. Nakanishi, T. Narumi, Y. Terada, and M. Tokuyama, *Rep. Inst. Fluid Science* **19**, 21 (2008).
- [25] D. M. Heyes and A. C. Brańka, *J. Chem. Phys.* **122**, 234504 (2005).
- [26] E. Kohira, Y. Terada, and M. Tokuyama, *Rep. Inst. Fluid Science* **19**, 91 (2007).
- [27] M. Tokuyama and Y. Terada, *Physica A* **375**, 18 (2007).
- [28] M. Tokuyama, *Phys. Rev. E* **62**, R5915 (2000).
- [29] T. A. Weber and F. H. Stillinger, *Phys. Rev. B* **31**, 1954 (1985).
- [30] X. J. Han and H. Teichler, *Phys. Rev. E* **75**, 061501 (2007).
- [31] A. Nakano, L. Bi, R. K. Kalia, and P. Vashishta, *Phys. Rev. B* **49**, 9441 (1994).
- [32] M. Hemmati and C. A. Angell, in *Physics Meets Geology*, edited by H. Aoki and R. Hemley (Cambridge University Press, Cambridge, England, 1998).
- [33] T. Narumi and M. Tokuyama, *Rep. Inst. Fluid Science* **19**, 73 (2007).